

Directional Carrier Transport in Micrometer-Thick Gallium Oxide Films for High-Performance Deep-Ultraviolet Photodetection

Wenrui Zhang,^{1,2*} Wei Wang,¹ Jinfu Zhang,¹ Tan Zhang,¹ Li Chen,¹ Liu Wang,¹ Yu Zhang,³ Yanwei Cao,¹ Li Ji,³ Jichun Ye^{1,2*}

¹ Zhejiang Provincial Engineering Research Center of Energy Optoelectronic Materials and Devices, Ningbo Institute of Materials Technology and Engineering, Chinese Academy of Sciences, Ningbo 315201, China

² Yongjiang Laboratory, Ningbo 315201, China

³ State Key Laboratory of ASIC and System, School of Microelectronics, Fudan University, Shanghai 200433, China

Keywords: ultraviolet photodetector, wide-bandgap semiconductor, gallium oxide, carrier transport, defect

Abstract

Incorporating emerging ultrawide bandgap semiconductors with a metal-semiconductor-metal (MSM) architecture is highly desired for deep-ultraviolet (DUV) photodetection. However, synthesis-induced defects in semiconductors complicate the rational design of MSM DUV photodetectors due to their dual role as carrier donors and trap centers, leading to a commonly observed trade-off between responsivity and response time. Here, we demonstrate a simultaneous improvement of these two parameters in ϵ -Ga₂O₃ MSM photodetectors by establishing a low-defect diffusion barrier for directional carrier transport. Specifically, using a micrometer thickness far exceeding its effective light absorption depth, the ϵ -Ga₂O₃ MSM photodetector achieves over 18-fold enhancement of responsivity and simultaneous reduction of the response time, which exhibits a state-of-the-art photo-to-dark current ratio near 10^8 , a superior responsivity of >1300 A/W, an ultrahigh detectivity of $>10^{16}$ Jones and a decay time of 123 ms. Combined depth-profile spectroscopic and microscopic analysis reveals the existence of a broad defective region near the lattice-mismatched interface followed by a more defect-free dark region, while the latter one serves as a diffusion barrier to assist frontward carrier transport for substantially enhancing the photodetector performance. This work reveals the critical role of the semiconductor defect profile in tuning carrier transport for fabricating high-performance MSM DUV photodetectors.

1. INTRODUCTION

Ultrawide-bandgap (UWBG) semiconductors exhibit competing characteristics for developing next-generation power electronics, ultraviolet photodetectors and sensors.¹⁻³ As an emerging UWBG material, gallium oxide (Ga_2O_3) possesses several appealing advantages for fabricating deep-ultraviolet (DUV) photodetectors, including an inherent wide bandgap (≥ 4.6 eV) with strong band-edge absorption, a simple binary composition, and a relatively long minority carrier diffusion length.^{4,5} As such, extensive research efforts are devoted to fabricating DUV photodetectors based on different forms of Ga_2O_3 , such as nanostructured Ga_2O_3 ,⁶ amorphous Ga_2O_3 ⁷⁻⁹, single-crystalline β -,¹⁰⁻¹² ϵ -,¹³⁻¹⁵ α - Ga_2O_3 thin films.¹⁶⁻¹⁸ and mixed-phase Ga_2O_3 .¹⁹⁻²¹ A majority of the above-mentioned DUV photodetectors adopt a planar metal-semiconductor-metal (MSM) device structure, as shown in Scheme 1a, owing to the simple device fabrication and feasible integration with external circuits.²²⁻²⁴ In a typical photodetection incident, photon collection and photocarrier transport are two essential steps (Scheme 1b), which are associated with the effective light absorption length (d_p) and the minority carrier diffusion length (d_h , hole in the Ga_2O_3 case), respectively. Accordingly, these two fundamental parameters provide key design guidelines for optimizing the structure geometry of MSM devices, including the film thickness (t_{film}) and the electrode spacing (t_{space}), in an effort to obtain maximum photodetector performance.

The principle for optimizing the MSM device geometry is to maximize photon collection and facilitate carrier collection. Compared to the straightforward role of t_{space} that mainly determines the transport distance, designing an appropriate t_{film} is relatively complicated as it relies on the trade-off between light absorption and carrier transport. In fact, very large inconsistency of the device parameters is seen in previous Ga_2O_3 MSM photodetector studies, where the reported optimized t_{film} values vary from 30 to 1000 nm.⁷⁻¹⁸ While such inconsistency is likely attributed to

different material qualities in these studies, it is not clear how the material defect affects the DUV photodetection behavior of a Ga₂O₃-based MSM photodetector, and how to coordinate the device's parameters for optimized performance. Particularly, a trade-off effect is commonly observed that relies on lattice defects as trap centers to enhance the photocurrent gain, which, however, inevitably compromises the response speed due to the slow de-trapping process.²⁵⁻²⁷ In this work, we perform a systematic study to understand how to design the device's geometric parameters with Ga₂O₃ characteristics and defects for fabricating high-performance MSM DUV photodetectors. It is discovered that adopting a micrometer thickness rather than a commonly suggested d_p simultaneously achieves more than 18-fold enhancement of responsivity and over 100% enhancement of the response speed in ϵ -Ga₂O₃ thin film MSM photodetectors. The simultaneous optimization of the responsivity and the response time is achieved via establishing an extra dark region in the micrometer-thick films as a diffusion barrier, which drives directional carrier transport to the front electrode for larger carrier collection efficiency in a non-trapped fast manner.

2. RESULTS AND DISCUSSION

2.1 Thin film growth and structure characterization

The 1%Sn-doped Ga₂O₃ (molar ratio, Sn-Ga₂O₃) films are grown using pulsed laser deposition (PLD) on c-plane single-crystal sapphire substrates. The Sn doping is critical to assist the formation of ϵ -Ga₂O₃ films rather than contributing excessive carriers in current synthesis conditions.²⁸ A range of laser pulse numbers from 600 (0.6kp) to 40000 (40kp) pulses is used to fabricate Ga₂O₃ films with various film thicknesses. The X-ray diffraction (XRD) results in Figure 1a show that all the films are crystallized as ϵ -Ga₂O₃ with a single set of (00 l) diffraction peaks in the out-of-plane direction. The film crystallinity increases at thicker films, as seen from the rocking curve measurements in Figure 1b. The full width at half maximum (FWHM) of the (004) ϵ -Ga₂O₃

peak decreases from 1.15 degree to 0.62 degree as the laser pulse number increases from 0.6kp to 40kp. The film thickness increases almost linearly with the pulse number (Figure S1), which is established by checking the cross-sectional specimens using the scanning electron microscopy (SEM). Figure 1c presents two representative SEM images for measuring the film thickness for 2kp and 20kp, which determines an average growth rate of 0.10-0.12 nm/pulse. The laser pulse number of as-deposited ϵ -Ga₂O₃ films is used in the following discussion to accurately label the film thickness.

The film microstructure is further characterized by transmission electron microscope (TEM) and energy-dispersive X-ray (EDX) mapping. It is observed uniform single-phase structure of the ϵ -Ga₂O₃ film from the cross-sectional scanning transmission electron microscopy (STEM) image and corresponding EDX maps in Figure 1d. The high-resolution TEM image in Figure 1e reveals a homogenous crystalline film lattice accompanied with a disordered interlayer region near the interface. Such interlayer region could help accommodate the large lattice mismatch between the film and the substrate, which is widely observed in previous reports.^{29,30} In addition to the decent phase purity and crystallinity, these ϵ -Ga₂O₃ films are quite smooth, exhibiting surface roughness (R_a) values of 0.49 nm (1.61 nm) for the 2kp (20kp) film (Figure 1f).

2.2 Thickness-dependent photodetector performance

Optical absorption measurements reveal sharp absorption edges and determine a direct optical bandgap of 4.9 ± 0.1 eV for ϵ -Ga₂O₃ (Figure 2a and Figure S2). Analysis of the absorption data of the 0.6kp film determines the absorption coefficients larger than 1.2×10^5 cm⁻¹ for the light with a wavelength $\lambda < 260$ nm, which is consistent with previous reports.³¹ This identifies a d_p value of ~200 nm that is close to the 2kp thickness, assuming more than 90% absorption of the incident light (Figure 2b). Since further thicker part may be treated as a dark region, the conventional design

strategy would expect a maximum photocurrent occurring near the 2kp thickness of the ϵ -Ga₂O₃ film. To testify this strategy, we prepare MSM photodetectors by depositing metallic Au/Ti electrodes on top of ϵ -Ga₂O₃ films with a specific finger spacing (500 μ m), length (150 μ m) and width (150 μ m). Surprisingly, it is observed that the photocurrent increases significantly even when t_{film} exceeds the 2kp value, while the dark current remains at an extremely low level below 10^{-12} A for all investigated film thicknesses. Under 254 nm illumination with an intensity of 4 mW/cm² and a bias of 20 V, a photocurrent over 3.0×10^{-5} A is obtained for ϵ -Ga₂O₃ photodetectors with t_{film} of 15kp and thicker ones, representing more than 18-fold enhancement than the 2kp film (Figure 2c). Similar thickness dependence of photocurrent is also seen with a much weaker light intensity of 20 μ W/cm² (Figure 2d and Figure S3), which demonstrates the reproductivity of this intriguing phenomenon under both strong and weak light conditions.

To fully understand the performance difference affected by t_{film} , we select ϵ -Ga₂O₃ photodetectors with two representative thicknesses of 2kp and 20kp for more comprehensive photoelectric characterization. Figure 3a and 3b present the current-voltage (I - V) curves of these two photodetectors under 254 nm illumination with various intensities from weak (4 μ W/cm²) to strong (9.3 mW/cm²). Both photodetectors present clear photoresponse for the investigated range of light intensity. A noticeable ON-OFF ratio of ~ 1000 remains for the 20kp photodetector even at a weak light intensity of 4 μ W/cm², implying decent capability for weak light detection. These two photodetectors both follow a linear power dependence with a $R^2 > 0.99$ for the entire intensity range (Figure 3c), exhibiting a broad linear dynamic range highly desired for practical light detection.³² The dynamic photoresponse of both photodetectors is relatively fast (Figure 3d and 3e). Based on the transient photoresponse to 254 nm illumination of 4 mW/cm², the 20kp photodetector delivers a rise time (t_{rise}) of 0.166 s and a fall time (t_{fall}) of 0.075 s, compared to

0.342s (t_{rise})/0.061s (t_{fall}) for the 2kp-thick photodetector. It is somewhat surprising that the thicker film achieves larger responsivity and an even faster rise time, compared to a more-commonly observed trade-off relation of these two metrics. The wavelength-dependent photoresponse of the ϵ -Ga₂O₃ photodetectors in Figure 3f exhibits good solar-blind photodetection behavior. A peak responsivity (R_p) is obtained near the wavelength of ~240 nm, and the 20kp photodetector gives a $R_p/R(400nm)$ rejection ratio of 1.87×10^4 .

2.3 Electrode spacing effect and photodetector optimization

Besides the film thickness t_{film} , the top electrode spacing (t_{space}) is another key design parameter that determines the carrier transport distance. Adjusting t_{space} towards the hole diffusion length d_h of Ga₂O₃ is helpful to shorten the transit distance and facilitate carrier collection. To optimize this parameter, we select the 20kp-thick ϵ -Ga₂O₃ film and fabricate MSM photodetectors with t_{space} varying from 1 μm to 200 μm , as shown in Figure 4a. The spacing of 1 μm is near the minimum feature size of the conventional lithography process, and 200 μm is among the largest electrode sizes used in most Ga₂O₃-based MSM photodetectors. The dark current remains relatively stable less than 5×10^{-12} A for all the spacings, reflecting ultralow point defect level for these ϵ -Ga₂O₃ films (Figure S4). By contrast, the photocurrent exhibits more apparent dependence on t_{space} (Figure 4b). The photodetector with $t_{space} = 1 \mu\text{m}$ exhibits a photocurrent of $\sim 1.1 \times 10^{-4}$ A, which is nearly 10 times larger than 1.3×10^{-5} A observed for $t_{space} = 150 \mu\text{m}$. This gives a state-of-the-art photo-to-dark current ratio (PDCR) of 9.49×10^7 . Incorporating the effective electrode area for the responsivity (detectivity) calculation, the ϵ -Ga₂O₃ photodetector with $t_{space} = 1 \mu\text{m}$ achieves a maximum responsivity (detectivity) of 1388 A/W (1.01×10^{16} Jones), which is the highest among previous reported MSM DUV photodetectors (Table S1).⁷⁻¹⁸ The response time is also affected by t_{space} , with much longer t_{rise} observed for smaller t_{space} (Figure 4c). Overall, as t_{space} increases, the

responsivity and detectivity decrease continuously (Figure 4d), which is accompanied by an obvious increase with the response speed, in particular for the rise time (Figure 4e). Such trade-off relation tuned by t_{space} is distinct from the relation by t_{film} , reflecting a fundamentally different role of the film thickness in assisting carrier transport.

2.4 Defect profile characterization

Since carrier transport is closely related to the defect density and distribution, we probe such information using depth profile X-ray photoelectron spectroscopy (XPS) to understand the key impact of the extra film thickness in heteroepitaxial $\epsilon\text{-Ga}_2\text{O}_3$ films on simultaneously enhancing the responsivity and the response speed. Using the 2kp film as a representative sample, we collect XPS spectra at regions from the top surface to the bottom substrate. The C $1s$ peak from the surface absorbed carbon and the Al $2p$ peak from the substrate are representative top and bottom signals for monitoring the etching process (Figure 5a). As a major defect indicator, the oxygen vacancy is widely analyzed from the deconvolution of the O $1s$ peak, which consists of a peak signal from the lattice oxygen near 530 eV and the oxygen vacancy signal near 532 eV.^{33,34} We start discussing the spectra evolution from an etching time of 300 s to avoid the complication of surface-absorbed hydroxides. For the 2kp film, it is observed clear peak broadening or appearance of an apparent peak shoulder near 532 eV with increasing etching time (Figure 5c), compared to much less variation of Ga $2p$ or Sn $3d$ peaks (Figure S5). Based on the etching distance, the width of this defective region is found larger than 100 nm starting from the substrate. Once the etched position arrives at the substrate, the O $1s$ peak becomes narrow again as the main contribution comes from the lattice oxygen in Al_2O_3 . We further perform the depth profile XPS analysis for the 20kp film using the same etching depth as 2kp, so that it mainly probes its top region (Figure 5b). The O $1s$ peak signal is found mainly from the lattice oxygen (Figure 5d), reflecting a uniform and more

defect-free top region. Stronger XPS signals for the Sn elements at the surface is seen from for both 2kp and 20kp films (Figure S5d), which again suggests a catalyst role of the Sn element in assisting the growth of the ϵ -Ga₂O₃.^{35,36}

The distinct defect distribution between the interface region and the top film provides valuable insights for understanding the dramatical enhancement of responsivity with faster response time occurring at a thickness far larger than d_p . It is well established that material defects, in the form of lattice disorders and surface defects, widely exist for films grown on heterogeneous substrates.^{37,38} This is particularly true for the film growth with large lattice mismatch, such as the case of ϵ -Ga₂O₃ on sapphire in this study. The STEM image in Figure 6a identifies a disordered interface region with a high density of misfit dislocations and domain boundaries, in particular for the initial 100-150 nm region, which is consistent with the XPS observation. Such defects do not form a conductive channel through the film, so that a similarly low level of dark current is observed for films with different thicknesses. In the thicker film region, many dislocations get annihilated or terminated which leads to larger domain size and higher film crystallinity (Figure S6). In a thin film case with $t_{film} \leq d_p$, the defective interface region largely overlaps with the light absorption region. Thus, a considerable amount of photocarriers are more easily trapped and recombined with free carriers in this region, which seriously compromises the device photocurrent (Figure 6b). By contrast, for thicker films ($t_{film} > d_p$), an extra dark region with higher crystallinity and less defect density is established, as observed in the case of the 20kp film. Such a dark region could hinder the backflow of photocarriers and drive them to diffuse towards the front contact, thus enhancing the carrier collection efficiency and the overall photocurrent (Figure 6c). Such diffusion-driven photocarrier transport is seen in semiconductors with large exciton binding energy and long minority carrier diffusion lengths, such as Ga₂O₃, ZnO, GaN and AlGaIn.³⁹⁻⁴³

A key advantage of this transport behavior is that the extra photocurrent gain presents less dependence on the formation of trap centers, and the directional carrier diffusion within the low-defect region could allow simultaneous optimization of the response speed. We note that this transport behavior is different from trap-assisted transport due to lattice disorders or surface defects that otherwise cause a trade-off between the responsivity and the response time. The latter phenomenon is actually seen in the optimization trend of t_{space} in this study, where surface defects likely play a more important role in dictating the photodetector performance at a smaller feature size. Figure 6d summarizes the key device metrics of our ϵ -Ga₂O₃ photodetector compared with previously reported state-of-the-art Ga₂O₃ MSM photodetectors, evidencing its superior performance in simultaneous achievement of a record high responsivity and PDCR, a low dark current, microsecond decay time and a decent UV-visible rejection ratio.

3. CONCLUSIONS

We have developed high-performance MSM DUV photodetectors based on heteroepitaxial ϵ -Ga₂O₃ films by establishing an extra dark region with a low defect density to significantly enhance carrier collection efficiency. The optimized micrometer-thick ϵ -Ga₂O₃ MSM photodetector achieves a record high PDCR of 9.48×10^7 and a responsivity of 1388 A/W, a relatively fast decay time of 123 ms, a pA dark current under a 20 V bias, and a UV-Vis rejection ratio of 1.87×10^4 . Combined TEM and depth profile XPS investigations reveal a broad defective region stemming from the ϵ -Ga₂O₃/Al₂O₃ interface, in neighboring with a more defect-free region in the upper portion of the ϵ -Ga₂O₃ film. The latter one becomes essential as a blocking layer between the photocarriers in the upper illumination area and the defect traps near the bottom interface. As such, the micrometer-thick ϵ -Ga₂O₃ films achieve maximum photocarrier collection, and obtain simultaneous optimization of the responsivity and the response time. This study offers a unique

perspective for engineering the defect profile in UWBG semiconductors with large minority carrier diffusivity for developing high-performance MSM DUV photodetectors.

4. METHODS

Thin film growth: The Sn-doped ϵ -Ga₂O₃ films with a 1% molar doping ratio were deposited on c-plane sapphire using pulsed laser deposition at a growth temperature of 750-800 °C and a dynamic oxygen pressure of 20 mTorr O₂. A 248 nm excimer laser source was used with a laser fluence of 1-2 J/cm² and a repetition rate of 2-5 Hz. After deposition, all the films were cooled down at 20 mTorr O₂ with a cooling rate of 20 °C/min. The film thickness was controlled by adjusting the laser pulse number.

Structural, chemical and optical characterization: The thin film phase, crystallinity and microstructure were investigated with high-resolution X-ray diffraction (XRD, Bruker D8 Advance) and transmission electron microscope (TEM, ThermoFisher Talos F200X) equipped with a Super-X energy-dispersive X-ray (EDX) analyzer. The film surface morphology was investigated using atomic force microscopy (AFM, Bruker Dimension Icon). The film thickness was mainly checked using the cross-sectional specimens by scanning electron microscopy (SEM, HITACHI Regulus-8230). The element oxidation state was characterized using X-ray photoemission spectroscopy (XPS, Kratos AXIS SUPRA) using Mg K_α (hν = 1253.6 eV) as the excitation source. For XPS depth profile measurement, an Ar⁺ ion sputtering source operated at a 4 kV voltage was used with an interval sputtering time of 300 seconds. The beam scan size is 4×4 mm² and the incident angle is 45 degree. Optical transmission spectra were collected with a UV-Vis/NIR Spectrophotometer (PerkinElmer, Lambda 950).

Photodetector fabrication and performance measurement: Photodetector devices with a metal-semiconductor-metal (MSM) structure are fabricated using e-beam evaporation by depositing a Au (50 nm)/Ti (20 nm) bilayer as the interdigital electrodes on top of the Ga₂O₃ films. The electrode spacing and the effective electrode area were controlled using a direct-write optical lithography machine (MicroWriter ML3) and a lift-off process. The photodetector performance was evaluated using a Keithley 4200 parameter analyzer connected with a probe station at ambient conditions. The incident light with variable intensities was calibrated with a standard UV-enhanced Si photodiode sensor. For spectral response measurement, monochromatic illumination was obtained from a 300 W Xenon lamp equipped with a monochromator. The calculation methods for

the photodetectors metrics, including responsivity, detectivity and response time, are described in references.^{4,5}

ASSOCIATED CONTENT

Supporting Information

The Supporting Information is available free of charge on the ACS Publications website.

Film thickness as a function of the laser pulse number for as-deposited ϵ -Ga₂O₃ films on sapphire. Tauc plot of the 2kp-thick ϵ -Ga₂O₃ film. Current-voltage (*I-V*) characteristics of the ϵ -Ga₂O₃ MSM photodetectors with different film thicknesses. . Dark *I-V* characteristics of the 20kp-thick ϵ -Ga₂O₃ MSM photodetectors with a t_{space} of 1 μ m, 2 μ m and 4 μ m. High-resolution XPS depth profile analysis of the Ga 2p and Sn 3d core levels for 2kp-thick and 20kp-thick ϵ -Ga₂O₃ films. TEM characterization results of the ϵ -Ga₂O₃ film from the bottom region to the top region showing the evolution of misfit dislocations and domain boundaries through the film thickness. A supporting table of performance comparison of reported MSM photodetectors based on planar Ga₂O₃ films with different Ga₂O₃ phases

AUTHOR INFORMATION

Corresponding Author

*E-mail (Wenrui Zhang): zhangwenrui@nimte.ac.cn

*E-mail (Jichun Ye): jjichun.ye@nimte.ac.cn

Notes

The authors declare no conflict of interest.

ACKNOWLEDGMENTS

This research was supported by Zhejiang Provincial Natural Science Foundation under Grant No. LZ21F040001, the Pioneer Hundred Talents Program of Chinese Academy of Sciences, Ningbo Yongjiang Talent Introduction Programme and Ningbo Key Scientific and Technological Project (Grant No. 2021Z083). Li Ji acknowledges the young scientist project of MOE innovation platform and State Key Laboratory of ASIC & System (2021MS004).

REFERENCES

1. Tsao, J. Y.; Chowdhury, S.; Hollis, M. A.; Jena, D.; Johnson, N. M.; Jones, K. A.; Kaplar, R. J.; Rajan, S.; Van de Walle, C. G.; Bellotti, E.; Chua, C. L.; Collazo, R.; Coltrin, M. E.; Cooper, J. A.; Evans, K. R.; Graham, S.; Grotjohn, T. A.; Heller, E. R.; Higashiwaki, M.; Islam, M. S.; Juodawlkis, P. W.; Khan, M. A.; Koehler, A. D.; Leach, J. H.; Mishra, U. K.; Nemanich, R. J.; Pilawa-Podgurski, R. C. N.; Shealy, J. B.; Sitar, Z.; Tadjer, M. J.; Witulski, A. F.; Wraback, M.; Simmons, J. A., Ultrawide-Bandgap Semiconductors: Research Opportunities and Challenges. *Adv. Electron. Mater.* **2018**, *4*, 1600501.
2. Guo, D.; Guo, Q.; Chen, Z.; Wu, Z.; Li, P.; Tang, W., Review of Ga₂O₃-Based Optoelectronic Devices. *Mater. Today Phys.* **2019**, *11*, 100157.
3. Pearton, S. J.; Yang, J.; CaryIV, P. H.; Ren, F.; Kim, J.; Tadjer, M. J.; Mastro, M. A., A Review of Ga₂O₃ Materials, Processing, and Devices. *Appl. Phys. Rev.* **2018**, *5*, 011301.
4. Chen, X.; Ren, F.; Gu, S.; Ye, J., Review of Gallium-Oxide-Based Solar-Blind Ultraviolet Photodetectors. *Photonics Res.* **2019**, *7*, 381-415.
5. Kaur, D.; Kumar, M., A Strategic Review on Gallium Oxide Based Deep-Ultraviolet Photodetectors: Recent Progress and Future Prospects. *Adv. Opt. Mater.* **2021**, *9*, 2002160.
6. Chen, X.; Liu, K.; Zhang, Z.; Wang, C.; Li, B.; Zhao, H.; Zhao, D.; Shen, D., Self-Powered Solar-Blind Photodetector with Fast Response Based on Au/ β -Ga₂O₃ Nanowires Array Film Schottky Junction. *ACS Appl. Mater. Interfaces* **2016**, *8*, 4185-4191.
7. Qin, Y.; Li, L.-H.; Yu, Z.; Wu, F.; Dong, D.; Guo, W.; Zhang, Z.; Yuan, J.-H.; Xue, K.-H.; Miao, X.; Long, S., Ultra-High Performance Amorphous Ga₂O₃ Photodetector Arrays for Solar-Blind Imaging. *Adv. Sci.* **2021**, *8*, 2101106.

8. Qian, L.-X.; Wu, Z.-H.; Zhang, Y.-Y.; Lai, P. T.; Liu, X.-Z.; Li, Y.-R., Ultrahigh-Responsivity, Rapid-Recovery, Solar-Blind Photodetector Based on Highly Nonstoichiometric Amorphous Gallium Oxide. *ACS Photonics* **2017**, *4*, 2203-2211.
9. Liu, N.; Zhang, T.; Chen, L.; Zhang, J.; Hu, S.; Guo, W.; Zhang, W.; Ye, J., Fast-Response Amorphous Ga₂O₃ Solar-Blind Ultraviolet Photodetectors Tuned by a Polar AlN Template. *IEEE Electron Device Lett.* **2022**, *43*, 68-71.
10. Arora, K.; Goel, N.; Kumar, M.; Kumar, M., Ultrahigh Performance of Self-Powered β -Ga₂O₃ Thin Film Solar-Blind Photodetector Grown on Cost-Effective Si Substrate Using High-Temperature Seed Layer. *ACS Photonics* **2018**, *5*, 2391-2401.
11. Zhang, X.; Wang, L.; Wang, X.; Chen, Y.; Shao, Q.; Wu, G.; Wang, X.; Lin, T.; Shen, H.; Wang, J.; Meng, X.; Chu, J., High-Performance β -Ga₂O₃ Thickness Dependent Solar Blind Photodetector. *Opt. Express* **2020**, *28*, 4169-4177.
12. Qian, L.-X.; Li, W.; Gu, Z.; Tian, J.; Huang, X.; Lai, P. T.; Zhang, W., Ultra-Sensitive β -Ga₂O₃ Solar-Blind Photodetector with High-Density Al@Al₂O₃ Core-Shell Nanoplasmonic Array. *Adv. Opt. Mater.* **2022**, *10*, 2102055.
13. Qin, Y.; Sun, H.; Long, S.; Tompa, G. S.; Salagaj, T.; Dong, H.; He, Q.; Jian, G.; Liu, Q.; Lv, H.; Liu, M., High-Performance Metal-Organic Chemical Vapor Deposition Grown ϵ -Ga₂O₃ Solar-Blind Photodetector With Asymmetric Schottky Electrodes. *IEEE Electron Device Lett.* **2019**, *40*, 1475-1478.
14. Qin, Y.; Li, L.; Zhao, X.; Tompa, G. S.; Dong, H.; Jian, G.; He, Q.; Tan, P.; Hou, X.; Zhang, Z.; Yu, S.; Sun, H.; Xu, G.; Miao, X.; Xue, K.; Long, S.; Liu, M., Metal-Semiconductor-Metal ϵ -Ga₂O₃ Solar-Blind Photodetectors with a Record-High Responsivity Rejection Ratio and Their Gain Mechanism. *ACS Photonics* **2020**, *7*, 812-820.

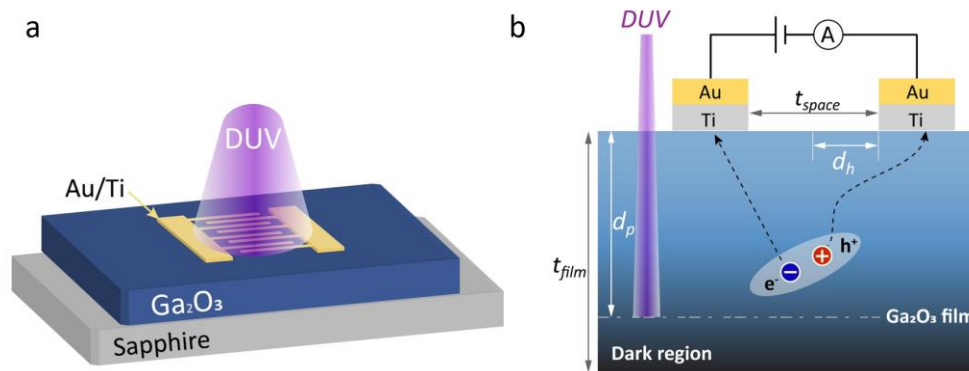
15. Li, S.; Yue, J.; Ji, X.; Lu, C.; Yan, Z.; Li, P.; Guo, D.; Wu, Z.; Tang, W., Oxygen Vacancies Modulating the Photodetector Performances in ϵ -Ga₂O₃ Thin Films. *J Mater. Chem. C* **2021**, *9*, 5437-5444.
16. Lee, S. H.; Lee, K. M.; Kim, Y.-B.; Moon, Y.-J.; Kim, S. B.; Bae, D.; Kim, T. J.; Kim, Y. D.; Kim, S.-K.; Lee, S. W., Sub-Microsecond Response Time Deep-Ultraviolet Photodetectors Using α -Ga₂O₃ Thin Films Grown via Low-Temperature Atomic Layer Deposition. *J. Alloys Compd.* **2019**, *780*, 400-407.
17. Qiao, G.; Cai, Q.; Ma, T.; Wang, J.; Chen, X.; Xu, Y.; Shao, Z.; Ye, J.; Chen, D., Nanoplasmonically Enhanced High-Performance Metastable Phase α -Ga₂O₃ Solar-Blind Photodetectors. *ACS Appl. Mater. Interfaces* **2019**, *11*, 40283-40289.
18. Sun, X.; Wang, Z.; Gong, H.; Chen, X.; Zhang, Y.; Wang, Z.; Yu, X.; Ren, F.; Lu, H.; Gu, S.; Zheng, Y.; Zhang, R.; Ye, J., M-Plane α -Ga₂O₃ Solar-Blind Detector With Record-High Responsivity-Bandwidth Product and High-Temperature Operation Capability. *IEEE Electron Device Lett.* **2022**, *43*, 541-544.
19. Guo, D. Y.; Chen, K.; Wang, S. L.; Wu, F. M.; Liu, A. P.; Li, C. R.; Li, P. G.; Tan, C. K.; Tang, W. H., Self-Powered Solar-Blind Photodetectors Based on α/β Phase Junction of Ga₂O₃. *Phys. Rev. Appl.* **2020**, *13*, 024051.
20. Wang, Y.; Cui, W.; Yu, J.; Zhi, Y.; Li, H.; Hu, Z.-Y.; Sang, X.; Guo, E.-j.; Tang, W.; Wu, Z., One-Step Growth of Amorphous/Crystalline Ga₂O₃ Phase Junctions for High-Performance Solar-Blind Photodetection. *ACS Appl. Mater. Interfaces* **2019**, *11*, 45922-45929.
21. Hou, X.; Zou, Y.; Ding, M.; Qin, Y.; Zhang, Z.; Ma, X.; Tan, P.; Yu, S.; Zhou, X.; Zhao, X.; Xu, G.; Sun, H.; Long, S., Review of Polymorphous Ga₂O₃ Materials and their Solar-Blind Photodetector Applications. *J. Phys. D: Appl. Phys.* **2021**, *54*, 043001.

22. Sarto, A. W.; Zeghbrock, B. J. V., Photocurrents in a Metal-Semiconductor-Metal Photodetector. *IEEE J. Quantum Electron.* **1997**, *33*, 2188-2194.
23. Soole, J. B. D.; Schumacher, H., InGaAs Metal-Semiconductor-Metal Photodetectors for Long Wavelength Optical Communications. *IEEE J. Quantum Electron.* **1991**, *27*, 737-752.
24. Xie, C.; Lu, X.-T.; Tong, X.-W.; Zhang, Z.-X.; Liang, F.-X.; Liang, L.; Luo, L.-B.; Wu, Y.-C., Recent Progress in Solar-Blind Deep-Ultraviolet Photodetectors Based on Inorganic Ultrawide Bandgap Semiconductors. *Adv. Funct. Mater.* **2019**, *29*, 1806006.
25. Zhou, H.; Cong, L.; Ma, J.; Li, B.; Xu, H.; Liu, Y., Suppression of Persistent Photoconductivity in High Gain Ga₂O₃ Schottky Photodetectors. *Chin. Phys. B* **2021**, *30*, 126104.
26. Jia, R.; Wu, X.; Deng, W.; Zhang, X.; Huang, L.; Niu, K.; Chi, L.; Jie, J., Unraveling the Mechanism of the Persistent Photoconductivity in Organic Phototransistors. *Adv. Funct. Mater.* **2019**, *29*, 1905657.
27. He, T.; Zhang, X.; Ding, X.; Sun, C.; Zhao, Y.; Yu, Q.; Ning, J.; Wang, R.; Yu, G.; Lu, S.; Zhang, K.; Zhang, X.; Zhang, B., Broadband Ultraviolet Photodetector Based on Vertical Ga₂O₃/GaN Nanowire Array with High Responsivity. *Adv. Opt. Mater.* **2019**, *7*, 1801563.
28. Zhang, W.; Zhang, J.; Chen, L.; Wang, W.; Zhang, T.; Liu, N.; Xu, T.; Yang, H.; Ye, J., Non-equilibrium Epitaxy of Metastable Polymorphs of Ultrawide-Bandgap Gallium Oxide. *Appl. Phys. Lett.* **2022**, *120*, 072101.
29. Xu, Y.; Park, J.-H.; Yao, Z.; Wolverton, C.; Razeghi, M.; Wu, J.; Dravid, V. P., Strain-Induced Metastable Phase Stabilization in Ga₂O₃ Thin Films. *ACS Appl. Mater. Interfaces* **2019**, *11*, 5536-5543.

30. Cora, I.; Mezzadri, F.; Boschi, F.; Bosi, M.; Čaplovičová, M.; Calestani, G.; Dódony, I.; Pécz, B.; Fornari, R., The Real Structure of ε -Ga₂O₃ and Its Relation to κ -phase. *CrystEngComm* **2017**, *19*, 1509-1516.
31. Passlack, M.; Schubert, E. F.; Hobson, W. S.; Hong, M.; Moriya, N.; Chu, S. N. G.; Konstadinidis, K.; Mannaerts, J. P.; Schnoes, M. L.; Zydzik, G. J., Ga₂O₃ Films for Electronic and Optoelectronic Applications. *J. Appl. Phys.* **1995**, *77*, 686-693.
32. Sanctis, A. D.; Jones, G. F.; Wehenkel, D. J.; Bezares, F.; Koppens, F. H. L.; Craciun, M. F.; Russo, S., Extraordinary Linear Dynamic Range in Laser-Defined Functionalized Graphene Photodetectors. *Sci. Adv.* **2017**, *3*, e1602617.
33. Dupin, J.-C.; Gonbeau, D.; Vinatier, P.; Levasseur, A., Systematic XPS Studies of Metal Oxides, Hydroxides and Peroxides. *Phys. Chem. Chem. Phys.* **2000**, *2*, 1319-1324.
34. Jia, M.; Wang, F.; Tang, L.; Xiang, J.; Teng, K. S.; Lau, S. P., High-Performance Deep Ultraviolet Photodetector Based on NiO/ β -Ga₂O₃ Heterojunction. *Nanoscale Res. Lett.* **2020**, *15*, 47.
35. Kracht, M.; Karg, A.; Schörmann, J.; Weinhold, M.; Zink, D.; Michel, F.; Rohnke, M.; Schowalter, M.; Gerken, B.; Rosenauer, A.; Klar, P. J.; Janek, J.; Eickhoff, M., Tin-Assisted Synthesis of ε -Ga₂O₃ by Molecular Beam Epitaxy. *Phys. Rev. Appl.* **2017**, *8*, 054002.
36. Kneiß, M.; Hassa, A.; Splith, D.; Sturm, C.; Wenckstern, H. v.; Schultz, T.; Koch, N.; Lorenz, M.; Grundmann, M., Tin-Assisted Heteroepitaxial PLD-Growth of κ -Ga₂O₃ Thin Films with High Crystalline Quality. *APL Mater.* **2019**, *7*, 022516.
37. Saadatkia, P.; Agarwal, S.; Hernandez, A.; Reed, E.; Brackenbury, I. D.; Coddling, C. L.; Liedke, M. O.; Butterling, M.; Wagner, A.; Selim, F. A., Point and Extended Defects in Heteroepitaxial β -Ga₂O₃ Films. *Phys. Rev. Mater.* **2020**, *4*, 104602.

38. Wang, Y.; Su, J.; Lin, Z.; Zhang, J.; Chang, J.; Hao, Y., Recent Progress on the Effects of Impurities and Defects on the Properties of Ga₂O₃. *J Mater. Chem. C* **2022**, *10*, 13395-13436.
39. Bechstedt, F.; Furthmüller, J., Influence of Screening Dynamics on Excitons in Ga₂O₃ Polymorphs. *Appl. Phys. Lett.* **2019**, *114*, 122101.
40. Yakimov, E. B.; Polyakov, A. Y.; Smirnov, N. B.; Shchemerov, I. V.; Yang, J.; Ren, F.; Yang, G.; Kim, J.; Pearton, S. J., Diffusion Length of Non-Equilibrium Minority Charge Carriers in β -Ga₂O₃ Measured by Electron Beam Induced Current. *J. Appl. Phys.* **2018**, *123*, 185704.
41. Zhang, W.; Yan, D.; Appavoo, K.; Cen, J.; Wu, Q.; Orlov, A.; Sfeir, M. Y.; Liu, M., Unravelling Photocarrier Dynamics beyond the Space Charge Region for Photoelectrochemical Water Splitting. *Chem. Mater.* **2017**, *29*, 4036-4043.
42. Cremades, A.; Albrecht, M.; Krinke, J.; Dimitrov, R.; Stutzmann, M.; Strunk, H. P., Effects of Phase Separation and Decomposition on the Minority Carrier Diffusion Length in Al_xGa_{1-x}N Films. *J. Appl. Phys.* **2000**, *87*, 2357-2362.
43. Karpov, S. Y.; Makarov, Y. N., Dislocation Effect on Light Emission Efficiency in Gallium Nitride. *Appl. Phys. Lett.* **2002**, *81*, 4721-4723.

Figures and captions



Scheme 1. (a) Schematic of a MSM photodetector for DUV light detection. (b) Schematic of a photodetection incident occurring in a MSM photodetector, which describes the key geometric parameters (film thickness t_{film} and electrode spacing t_{space}) along with the material characteristics (effective light absorption length d_p and the minority carrier diffusion length d_h).

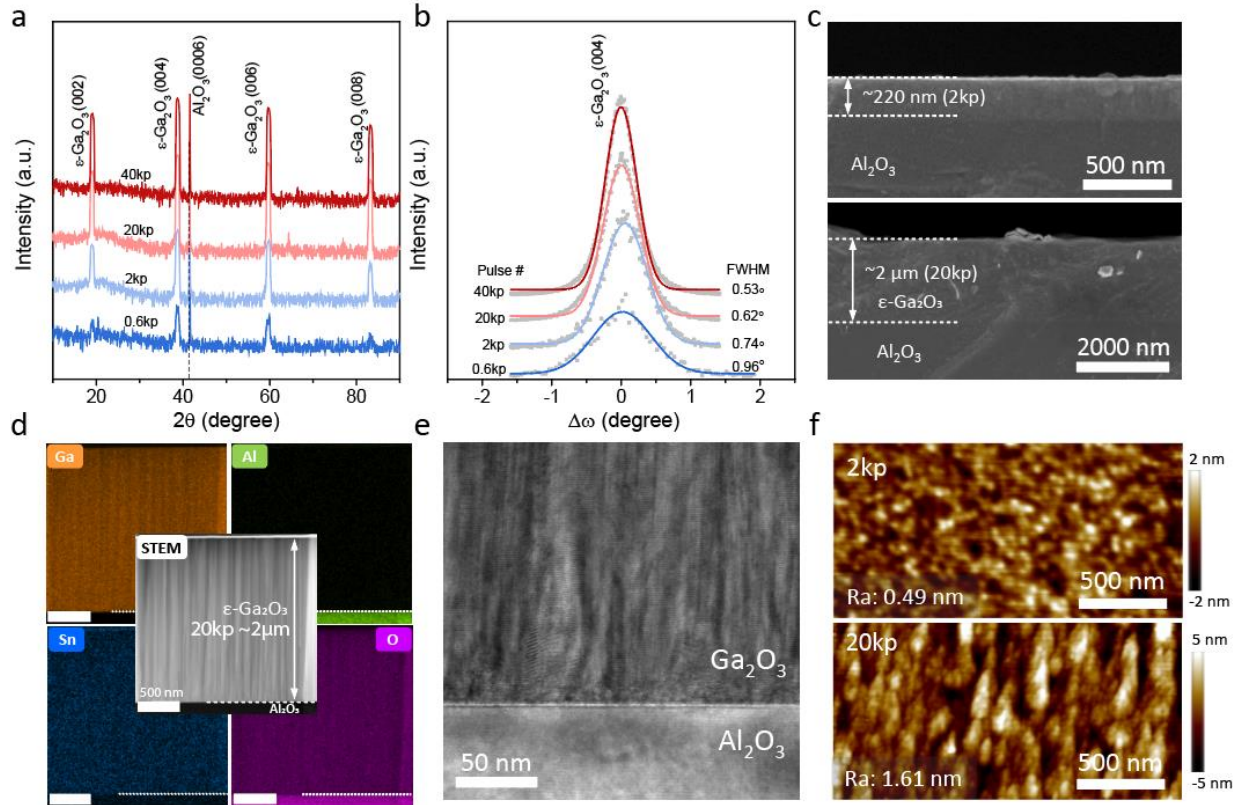


Figure 1. (a) θ -2 θ XRD full scans and (b) rocking curve profiles of Sn-doped ϵ - Ga_2O_3 films with different film thicknesses grown on c-plane sapphire. Gaussian fitting described by the line plot is used to determine the FWHM value of the rocking curve data described by scattered points. (c) Cross-sectional SEM images of ϵ - Ga_2O_3 films with pulse numbers of 2kp and 20kp for the thickness measurement. (d) Cross-sectional HAADF-STEM image of the 20kp ϵ - Ga_2O_3 film and corresponding EDX maps for Ga, Al, Sn, O elements in the same region. (e) High-resolution TEM image of the ϵ - Ga_2O_3 film near the film-substrate interface showing a homogenous film lattice and an abrupt interface. (f) AFM images of the 2kp-thick and 20kp-thick films shows a smooth surface morphology.

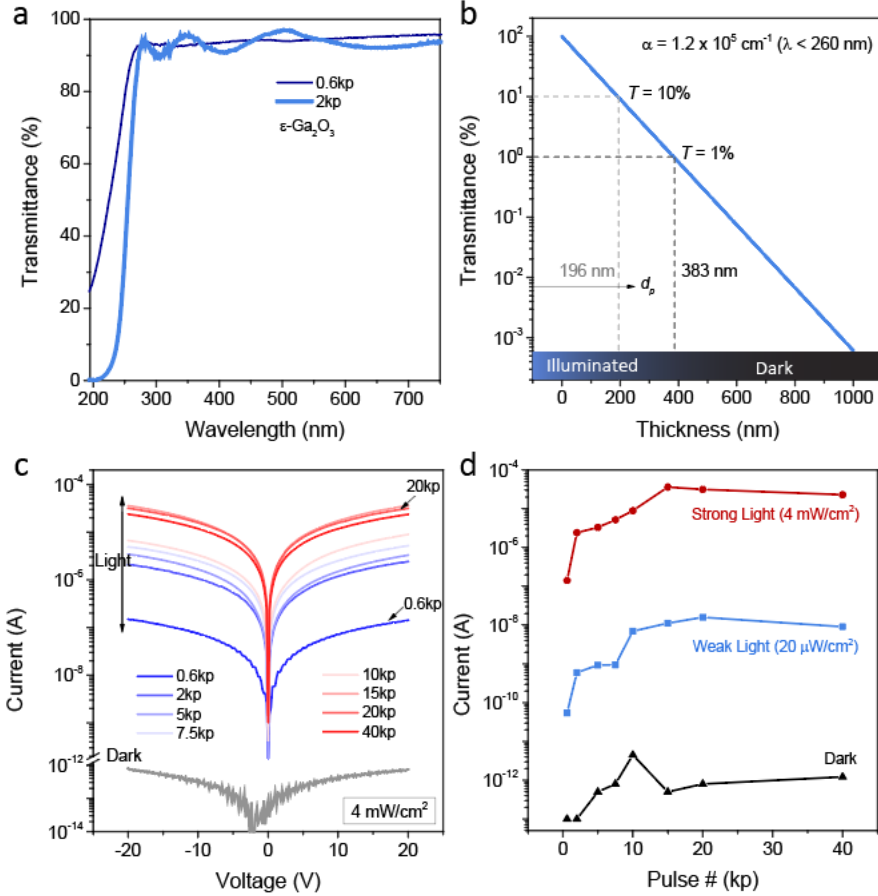


Figure 2. (a) Transmission spectra of the 0.6kp-thick and 2kp-thick ϵ -Ga₂O₃ films. (b) Thin film transmission as a function of the ϵ -Ga₂O₃ film thickness for the incident light with $\lambda < 260$ nm. (c) Current-voltage characteristics of the ϵ -Ga₂O₃ MSM photodetectors with different film thicknesses under 254 nm illumination with a light intensity of 4 mW/cm^2 . The dark current of the 20kp-thick device is plotted as a comparison. (d) Photocurrent as a function of the pulse number at strong and weak light conditions, with corresponding dark current for comparison.

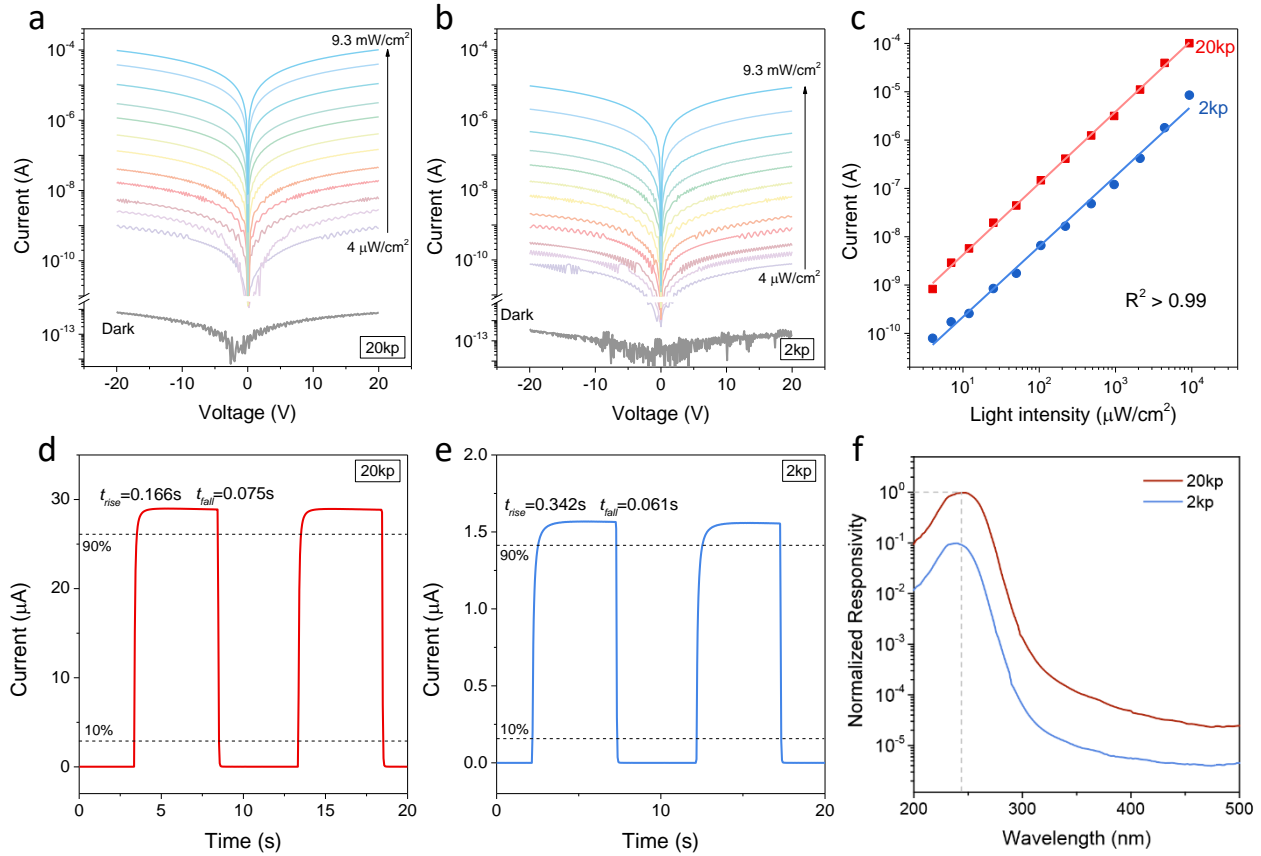


Figure 3. Current-voltage characteristics of (a) 20kp-thick and (b) 2kp-thick ϵ - Ga_2O_3 MSM photodetectors under different light intensities with corresponding dark current for comparison. (c) Photocurrent under a 20 V bias as a function of light intensity for 20kp-thick and 2kp-thick ϵ - Ga_2O_3 photodetectors. Current-time characteristics of (d) 20kp-thick and (e) 2kp-thick ϵ - Ga_2O_3 photodetectors under ON/OFF modulated illumination measured at 20 V for the dynamic response and reproductivity evaluation. The monochromatic illumination source has a wavelength of 254 nm and an intensity of 4 mW/cm^2 . (f) Wavelength-dependence responsivity at 20 V for 20kp-thick and 2kp-thick ϵ - Ga_2O_3 photodetectors. The responsivity values are normalized based on the peak responsivity of the 20kp-thick ϵ - Ga_2O_3 photodetector.

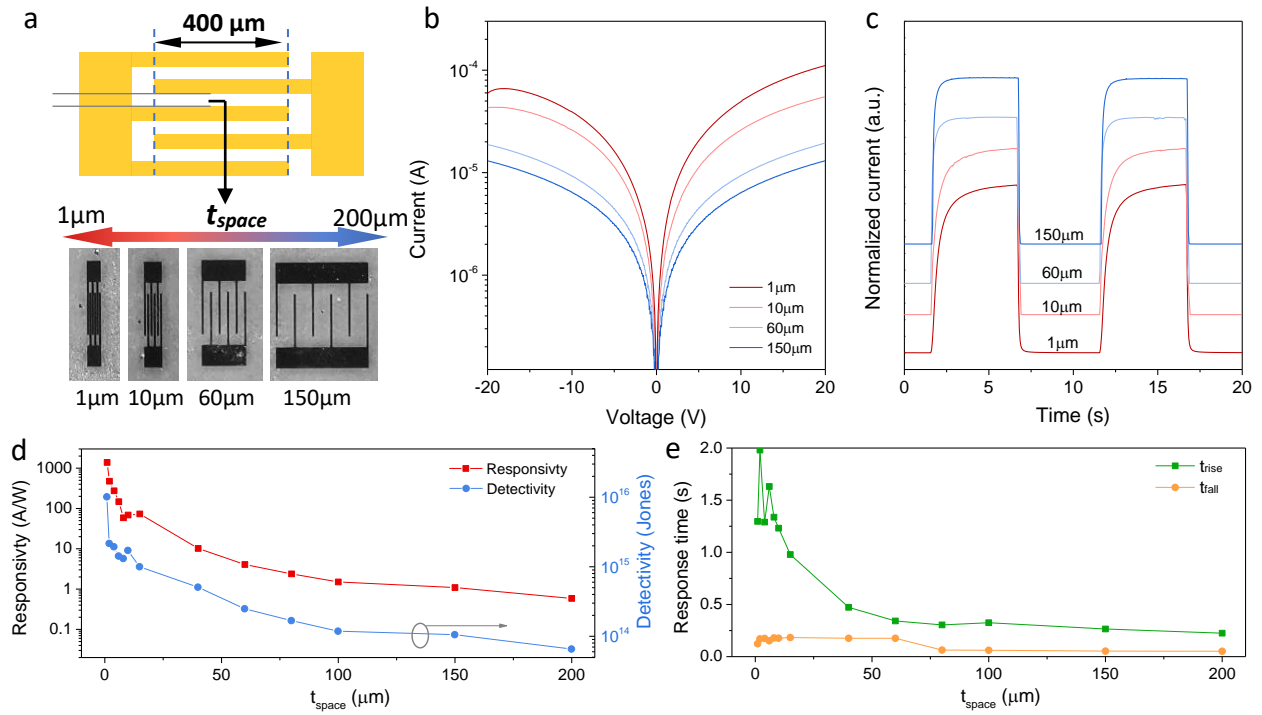


Figure 4. (a) Schematic of an interdigitated electrode design (upper) and corresponding optical images with variable t_{space} (lower). (b) Current-voltage and (c) current-time characteristics of 20kp-thick $\epsilon\text{-Ga}_2\text{O}_3$ MSM photodetectors with four different t_{space} of 1 μm , 10 μm , 60 μm and 150 μm measured with a light intensity of 4 mW/cm^2 . (d) Responsivity (left axis) and detectivity (right axis) and (e) response time as a function of t_{space} from 1 μm to 200 μm for the 20kp-thick $\epsilon\text{-Ga}_2\text{O}_3$ MSM photodetector.

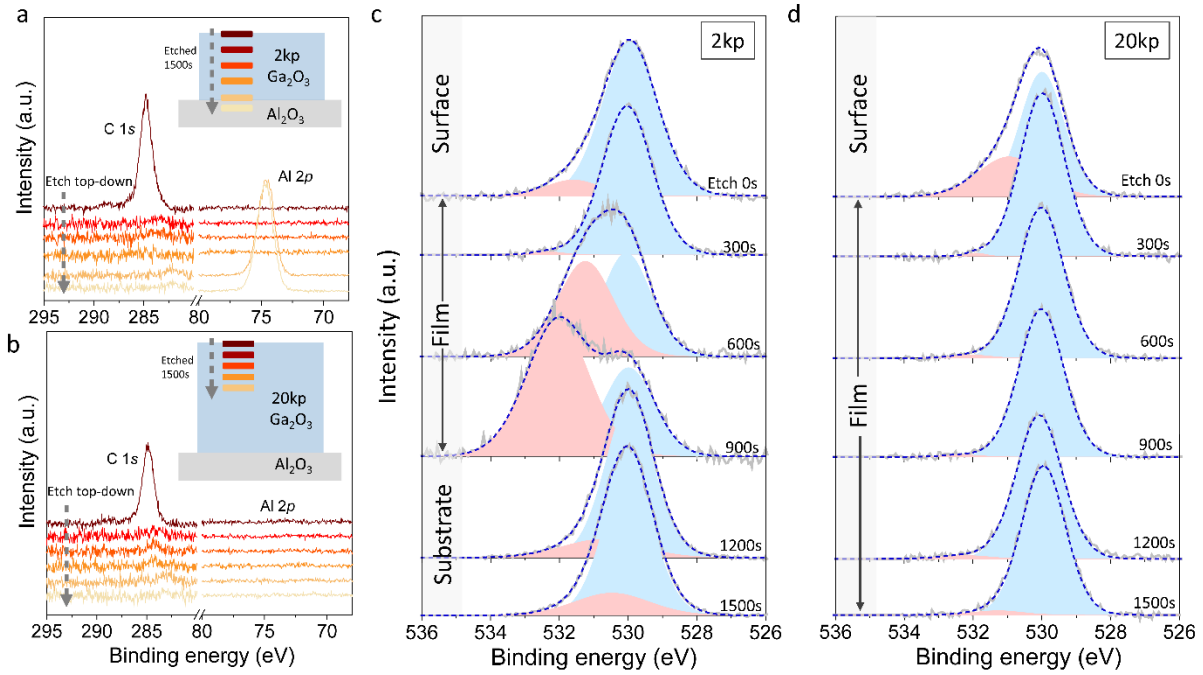


Figure 5. High-resolution C *1s* and Al *2p* XPS spectra collected at different etched depths for (a) 2kp- and (b) 20kp-thick ϵ -Ga₂O₃ films. The sputtering ion etching and data collection interval is 300 s, and the total etching time is 1500 s for both films. The depth profile analysis of the O *1s* core level for (c) 2kp- and (d) 20kp-thick ϵ -Ga₂O₃ films using the same etching depth, which respectively covers the entire film region for the 2kp film and only the top film region for the 20kp film.

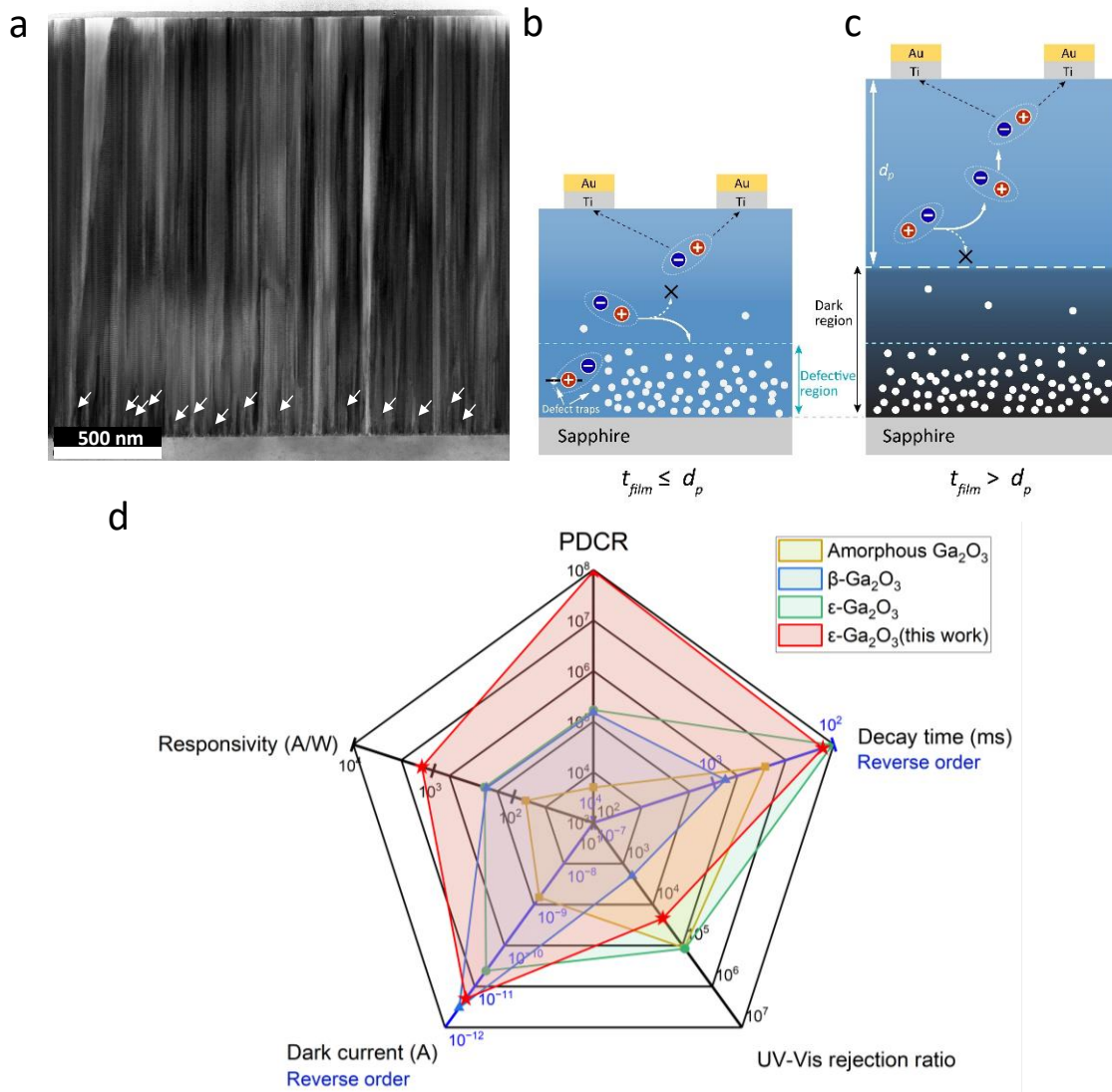


Figure 6. (a) Cross-sectional bright-field STEM image of a 20kp-thick ϵ - Ga_2O_3 film showing the formation of a defective region featured by a high density of misfit dislocations near the interface, followed by dislocation annihilation and domain broadening in the thicker region. Schematic of photocarrier transport for (b) $t_{film} \leq d_p$ and (c) $t_{film} > d_p$ in the ϵ - Ga_2O_3 MSM thin film photodetectors illustrating the critical role of the extra dark region in assisting carrier collection. (d) Radar plot summarizing critical device metrics of the ϵ - Ga_2O_3 MSM photodetector of this study compared with previous high-performance Ga_2O_3 MSM photodetectors based on different Ga_2O_3 phases.